Phase separated characteristics and soft magnetic properties of [Cu$_{0.6}$(FeCrC)$_{0.4}$]$_{100-x}$Si$_x$ immiscible composites by laser induction hybrid cladding

CrossMark

Shengfeng Zhou [a], Xiaoqin Dai [a, *], Chunxia Wang [b], Min Xie [a], Jiaoxi Yang [c, **], Zhengyang Li [d, ***]

[a] Laser Technology Institute, Tianjin Polytechnic University, Tianjin, 300387, PR China
[b] School of Materials Science and Engineering, Nanchang Hangkong University, Nanchang, Jiangxi 330063, PR China
[c] Institute of Laser Engineering, Beijing University of Technology, Beijing, 100124, PR China
[d] Institute of Mechanics, Chinese Academy of Sciences, Beijing 10090, PR China

ARTICLE INFO

ABSTRACT

The effect of Si addition on phase separation and soft magnetic properties of [Cu$_{0.6}$(FeCrC)$_{0.4}$]$_{100-x}$Si$_x$ (x = 3 and 8) immiscible composites produced by laser induction hybrid cladding (LIHC) has been investigated. The duplex structure of immiscible composites was composed of many Fe-rich particles dispersed within Cu-rich upper layer and large amounts of Cu-rich particles embedded within Fe-rich lower layer. However, the increasing Si addition not only induced the precipitation of intermetallic compound Cu$_{6.69}$Si within Cu-rich upper layer, but also increased the area of Fe-rich layer, the size of Fe- and Cu-rich particles, as well as the solubility of Si in Fe- and Cu-rich phases. Moreover, the micro-hardness of Fe- and Cu-rich layers was increased to 747.3HV$_{0.2}$ and 302.6HV$_{0.2}$ in the Cu$_{55.2}$(FeCrC)$_{36.8}$Si$_8$ immiscible composite, respectively, which was ~1.6 and ~1.8 times higher than that in the Cu$_{58.2}$(FeCrC)$_{38.8}$Si$_3$ immiscible composite, due to solid-solution strengthening and dispersion strengthening. Compared to the Cu$_{58.2}$(FeCrC)$_{38.8}$Si$_3$ immiscible composite, the Cu$_{55.2}$(FeCrC)$_{36.8}$Si$_8$ immiscible composite presented a saturated magnetization of 13.7 emu/g, relatively lower coercivity of 24.9 Oe and higher Curie temperature of larger than 400 K due to appearance of ferromagnetic α-Fe(Si) phase.

1. Introduction

When Cu-Fe immiscible alloys are supercooled to a certain temperature below the metastable liquid miscibility gap (T$_{sep}$), the melt can separate into two melts as a result of liquid phase separation: a Fe-rich melt (L1) and a Cu-rich melt (L2) [1,2]. The Cu-Fe immiscible alloys have become potential materials for electronic packaging solders, soft magnetic materials, electrical contact materials, and magnetoresistive materials if the spherical particles as the minor phase can be well dispersed in the metallic matrix [3]. However, the Stokes motion induced by the density difference

between the L1 and L2 results in macroscopic segregation due to gravity effect, which limits the wide application of the Cu-Fe immiscible alloys [4].

Generally, once liquid phase separation occurs, the L1 and L2 will not only experience their own supercooling, but also follow a solidification path that differs considerably from that expected for the bulk composition [5]. Much work about the formation mechanism of the LPS has also illustrated that the microstructure of the Cu-Fe immiscible alloys is mainly determined by alloy composition, supercooling, cooling rate and fluid flow during solidification [2,6]. Therefore, many methods have been proposed aimed specifically at improving the microstructure of Cu-Fe immiscible alloys, such as adding different alloy elements (Al [7], Si [8], Ni [9], Nd [10] and Ge [11]) and adopting high supercooling techniques (glass fluxing [12] and electromagnetic levitation [13]). Even under microgravity condition required to overcome the gravity effect on the macroscopic segregation, the collision and coalescence of minority phase

droplets can not be eliminated completely, implying that the rapid phase growth and coagulation are essentially unavoidable [14].

Compared to conventional solidification techniques, the rapid solidification can obtain cooling rate as high as 10^5 K/s, which, in turn, can lead to considerable dynamic supercooling, microstructure refinement, and extension of solid solubility [5]. Especially, when Wang et al. [15] produced the core-shell or egg-type microstructure in the Cu-Fe-Si powder by gas atomization, the Cu-Fe immiscible alloys were of particular interest for practical applications because iron had relatively lower cost than other metals such as Ag, Cr and Nb. For example, Koziel et al. [16] and Nagase et al. [17] found that large amounts of spherical fcc-Cu crystalline globules have been precipitated in a melt spun Fe-Cu-based immiscible alloys which contained a Fe-rich amorphous phase. Fu et al. [18] produced the nanostructured $Fe_{60}Cu_{40}$ (ratio of atom) immiscible alloy by a combustion synthesis combining rapid solidification, and found that the $Fe_{60}Cu_{40}$ immiscible alloy was composed of Fe-rich dendrite (a few micron) embedded in Cu-rich matrix uniformly (~30 nm) with a fractured strength of 1100 MPa and a Vicker's microhardness of ~2.5 GPa.

Recently, laser induction hybrid cladding (LIHC) was used to produce the Cu-Fe immiscible composites. It was found that the microstructure and properties not only depended on the inoculant addition of CNTs [19], alloying element addition of Al [7], but also on the substrate type and the laser scanning speed [20,21]. Moreover, the previous researches showed that the addition of Si to Cu-Fe immiscible alloys can improve the sensitivity of liquid/liquid phase separation, which results in a wide immiscible gap at temperature as high as 1723 K [8,22]. Therefore, the addition of low Si content (2 wt% [23] and 4 wt% [24]) to Cu-Fe-based immiscible alloys can refine the primary α-Fe microstructure and induce the secondary separated phases with high hardness. However, when the addition of Si to Cu-Fe-based immiscible alloys is further increased during LIHC, the microstructure and properties have not been reported. In the present paper, the Si contents (3 wt% and 8 wt%) are added into the Cu-Fe-based immiscible alloys produced by LIHC, the phase separation characteristics and soft magnetic properties are investigated.

2. Experimental procedures

The substrate used was low carbon steel with dimensions of 120 mm × 60 mm × 5 mm. The cladding powder was composed of pure copper powder (99.99%), Fe-based alloy powder (Fe-8.5Cr-0.5C) and pure Si powder (99.99%), whose particle size was 40 μm, 45 μm and 35 μm, respectively. The cladding powder with chemical compositions (wt.%) of $[Cu_{0.6}(FeCrC)_{0.4}]_{100-x}Si_x$ (x = 3 and 8) were

produced by mechanical milling at a rotary speed of 100 rpm for 2 h. The processing apparatus of the laser induction hybrid cladding has been described in detail previously [25]. The processing parameters were as follows: laser powder 5 kW, laser scanning speed 3500 mm/min, spot diameter 4 mm, overlapping rate 50%, powder feeding rate 96.2 g/min, angle between the powder nozzle and the substrate 53°, and the preheated temperature of the substrate 1173 K by adjusting the power of the induction heater. A shield of Ar gas was used to blow the cladding powder into the molten pool and shield the molten pool. The dimensions of the immiscible composites was 90 mm × 30 mm × 1.0 mm.

After LIHC, the metallurgical samples were mounted into epoxy resin, polished mechanically, and then etched by a solution with ratio of $FeCl_3$:HCl:H_2O = 10 g:25 mL:100 mL. Microstructure was examined by X-ray diffraction (XRD, Brucker D8 Advance) with Cu Kα radiation, scanning electron microscope (SEM, FEI Quanta 200, Netherlands) with energy dispersive X-ray spectroscopy (EDS), and transmission electron microscopy (TEM, JEOL 2100F at 200 kV), respectively. Microhardness of immiscible composite was tested by a Vickers-1000 tester using a load of 1.96 N and a dwelling time of 30 s. Magnetic properties were measured repeatedly by an MPMS XL vibrating sample magnetometer at room temperature with a maximum applied field of 20,000 Oe. The temperature dependence of magnetization curve was determined by heating the immiscible composites in the range of 1.9–400 K at 500 Oe.

3. Results

Fig. 1 shows the results of XRD patterns of the immiscible composites. When the Si addition is 3 wt%, the immiscible composite is mainly composed of face-centered cubic (fcc) ε-Cu and body-centered cubic (bcc) α-Fe. When the Si addition is increased to 8 wt%, the immiscible composite consists of fcc ε-Cu, bcc α-Fe and $Cu_{6.69}Si$ with a hexagonal structure. Obviously, the increasing Si content results in the intermetallic compound (IMC).

Fig. 2 shows the geometrical profiles of the immiscible composites. Due to liquid phase separation, the duplex structure is formed. According to the results of XRD and EDS, the lower layer is composed of Fe-rich matrix and the upper layer is composed of Cu-rich matrix (Fig. 2a and b). The concave morphologies are also observed at the interface of the lower and upper layers, implying that the violent convection and stirring occur during LIHC. Moreover, when the Si content is increased from 3 wt% to 8 wt%, the area of Fe-rich layer is also increased from 56.6% to 62.7% (Fig. 2c), indicating that the Si content plays an important role in the duplex structure.

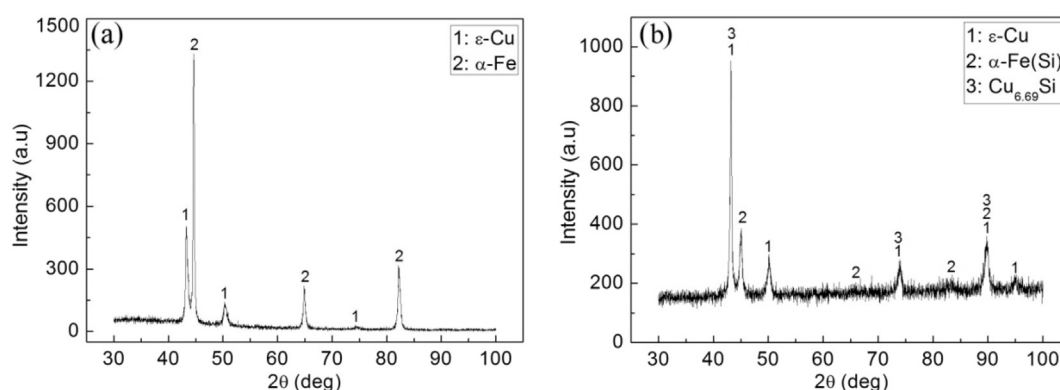Fig. 3 shows the microstructure of the $Cu_{58.2}(FeCrC)_{38.8}Si_3$

Fig. 1. X-ray diffraction patterns of the immiscible composites containing different Si contents: (a) 3 wt% Si, (b) 8 wt% Si.
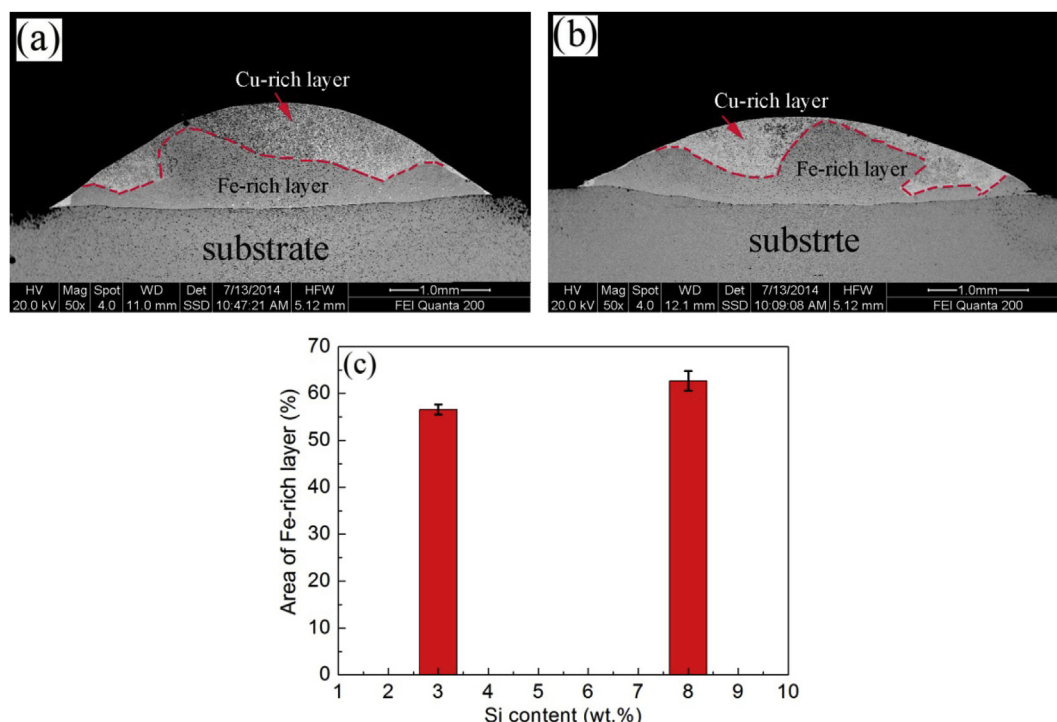
Fig. 2. Cross-sectional morphologies of the immiscible composites with different Si contents: (a) 3 wt% Si, (b) 8 wt% Si, (c) relationship between Si content and area of Fe-rich layer in the immiscible composite.

immiscible composite. According to the results of XRD and EDS (Table 1), the dendrite is identified as α-Fe containing a supersaturated Cu (12.7 wt%) and small amounts of Cr (7.2 wt%) and Si (2.44 wt%). Many spherical Cu-rich particles containing a supersaturated Fe (16.3 wt%) are embedded within the α-Fe interdendrites (Fig. 3a and b) and they have an average diameter of ~3.4 μm (Fig. 5). However, large amounts of spherical Fe-rich particles are dispersed within the Cu-rich matrix in the upper layer (Fig. 3c). These Fe-rich particles containing a supersaturated Cu (16.34 wt%), small amounts of Cr (5.77 wt%) and Si (3.25 wt%) have an average diameter of ~3.5 μm (Fig. 5). Additionally, large amounts of white nano-scaled Cu-rich grains are precipitated inside the Fe-rich particles due to the secondary liquid phase separation [5], as shown in Fig. 3d. The Cu-rich matrix in the upper layer contains 92.81 wt% Cu and 7.19 wt% Fe, which has a similar composition to the Cu-rich particles in the lower layer. According to the TEM bright field image and selected area electron diffraction (SAED) patterns (Fig. 3e and f), the nano-scaled Fe-rich particle is confirmed to be α-Fe phase with $(2\overline{2}0)$ and $(0\overline{2}4)$ planes and the Cu-rich matrix is confirmed to be ε-Cu phase with $(00\overline{2})$ and (020) planes.

Fig. 4 shows the microstructure of the $Cu_{55.2}(FeCrC)_{36.8}Si_8$ immiscible composite. Large amounts of spherical Cu-rich particles are also dispersed within the α-Fe interdendrites in the lower layer (Fig. 4a and b). According to the result of EDS analysis (Table 1), these Cu-rich particles contain 11.47 wt% Fe, 2.27 wt% Cr and 5.04 wt% Si. The α-Fe dendrites also contain a supersaturated Cu (7.11 wt%), 6.75 wt% Cr and large amounts of Si (10.36 wt%). These Cu-rich particles have a relatively larger diameter (~6.8 μm) compared to that in the $Cu_{58.2}(FeCrC)_{38.8}Si_3$ immiscible composite (Fig. 5). However, large amounts of impinging Fe-rich particles are dispersed within the Cu-rich matrix in the upper layer (Fig. 4c). The Fe-rich particle contains a supersaturated Cu (7.81 wt%), small amounts of Cr (9.52 wt%) and large amounts of Si (17.44 wt%) and has a diameter of ~10 μm. The Cu-rich matrix contains a

supersaturated Fe (4.26 wt%) and small amounts of Si (2.89 wt%). Interestingly, large amounts of white petal-like precipitations are formed on the Cu-rich matrix (Fig. 4d). These precipitations contain 65.41 wt% Cu, 24.21 wt% Fe, 3.21 wt% Cr and 7.08 Si. According to the TEM bright field image and SAED patterns (Fig. 4e and f), the petal-like precipitation is confirmed to be hexagonal $Cu_{6.69}Si$ with $(\overline{1}01)$ and $(1\overline{1}1)$ planes, the spherical Fe-rich particle is bcc α-Fe with $(00\overline{2})$ and $(\overline{1}31)$ planes and the Cu-rich matrix is fcc ε-Cu phase with $(\overline{1}1\overline{1})$ and $(\overline{1}11)$ planes.

Fig. 6 shows the microhardness distribution of the immiscible composites and pure Cu produced by LIHC. The immiscible composites have a sharply gradient distribution of microhardness, which is consistent with the duplex structure. For the $Cu_{58.2}(FeCrC)_{38.8}Si_3$ immiscible composite, the Fe-rich lower layer has an average microhardness of $472.8HV_{0.2}$, which is ~2.8 times higher than the Cu-rich upper layer ($165.5HV_{0.2}$). The microhardness of the Cu-rich layer is higher than that of pure Cu produced using LIHC ($104HV_{0.2}$). When the Si content is increased to 8 wt%, the microhardness of the Fe- and Cu-rich layers is increased to $747.3HV_{0.2}$ and $302.6HV_{0.2}$, respectively, which is ~1.6 and ~1.8 times higher than that of Fe- and Cu-rich layers in the $Cu_{58.2}(FeCrC)_{38.8}Si_3$ immiscible composite, respectively. Obviously, the increasing Si content can enhance the microhardness of the immiscible composites significantly.

Fig. 7 shows the magnetic hysteresis loops of the immiscible composites at 300 K. For the $Cu_{58.2}(FeCrC)_{38.8}Si_3$ immiscible composite, the magnetization can not reach a saturated state when the applied field is up to 20,000 Oe. The maximum magnetization is only ~2.3 emu/g and the coercivity is ~166.9 Oe (Fig. 7a). For the $Cu_{55.2}(FeCrC)_{36.8}Si_8$ immiscible composite, the saturated magnetization (~13.7 emu/g) can be obtained sharply when the applied field is only larger than 5000 Oe. The coercivity is only ~24.9 Oe (Fig. 7b). It indicates that the increasing Si content can also improve the soft magnetic properties of the immiscible composites.
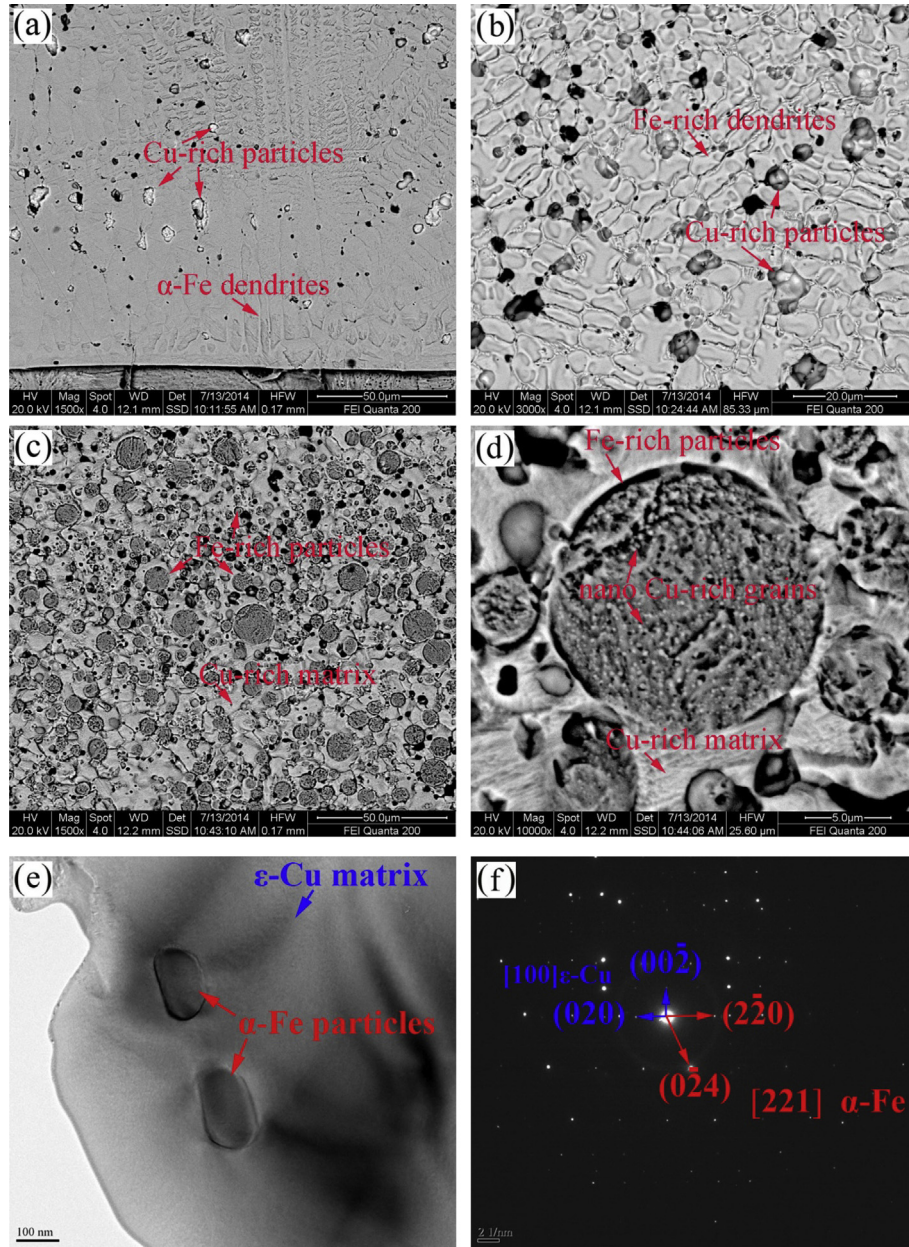
Fig. 3. (a) Microstructure of Fe-rich layer in the $Cu_{58.2}(FeCrC)_{38.8}Si_3$ immiscible composite, (b) magnified image of (a), (c) microstructure of Cu-rich layer in the immisicible composite, and (d) magnified image of (c), (e) TEM images and (f) SAED patterns of the immiscible composite.

Table 1
Chemical composition of the immiscible composites with different Si contents.

Immiscible composites	Cu-rich particle				Fe-rich matrix			
$Cu_{58.2}(FeCrC)_{38.8}Si_3$	Fe	Cr	Si	Cu	Cu	Cr	Si	Fe
	16.3	0	0	Bal.	12.7	7.2	2.44	Bal.
	Fe-rich particle				Cu-rich matrix			
	Cu	Cr	Si	Fe	Fe	Cr	Si	Cu
	16.34	5.77	3.25	Bal.	7.19	0	0	Bal.
$Cu_{55.2}(FeCrC)_{36.8}Si_8$	Cu-rich particle				Fe-rich matrix			
	Fe	Cr	Si	Cu	Cu	Cr	Si	Fe
	11.47	2.27	5.04	Bal.	7.11	6.75	10.36	Bal.
	Fe-rich particle				Cu-rich matrix			
	Cu	Cr	Si	Fe	Fe	Cr	Si	Cu
	7.81	9.52	17.44	Bal.	4.26	0	2.89	Bal.

4. Discussion

It has shown that the cooling rate of LIHC is of order of 10^4–10^5 K/s [21,25], which, in turn, can lead to extension of solid solubility, such as a supersaturated Cu in Fe or a supersaturated Fe in Cu, and considerable dynamic supercooling of ~150 K. Generally, the supercooling of the Cu-Fe immiscible alloys containing 40–65 wt% Cu is only 80–100 K if the liquid phase separation occurs [26]. Therefore, the $Cu_{58.2}(FeCrC)_{38.8}Si_3$ and $Cu_{55.2}(FeCrC)_{36.8}Si_8$ immiscible alloys can be supercooled readily below the T_{sep} and separate into the two melts: a Fe-rich melt as the minor phase (L1) and a Cu-rich melt as the major phase (L2). Subsequently, the L1 and L2 will follow their own solidification path to finish nucleation and growth. Generally, the critical nucleation work ΔG^*, can be given as follows [27]:

$$\Delta G^* = \frac{16\pi}{3} \frac{\sigma^3}{\Delta G_v^2} f(\theta) \qquad (1)$$

where σ, ΔG_v and $f(\theta)$ are the interfacial energy, the Gibbs free energy difference between solid and liquid, and catalytic factor for heterogeneous nucleation, respectively. According to the Cu-Fe binary phase diagram [28], the L1 has a relatively lower formation work for nucleation ΔG^* and has a good wettability with the Fe-substrate [20], the L1 can sink towards the bottom of the melt pool and solidify before the L2. As a result, the Fe-rich layer will form at the bottom of the melt pool and the Cu-rich layer will solidify on the surface of the solidified Fe-rich layer, resulting in the duplex structure (Fig. 2a and b).

During LIHC, the laser energy is consumed in three aspects: (1) melting the composite powder; (2) melting the substrate to form the melt pool; and (3) thermal radiation and the other loss. An energy balance for LIHC can expressed as follows [29,30]:

$$P = P_p + P_s + P_L \qquad (2)$$

where P is the laser power, P_p is the power used to melt the composite powder, P_s is the power used to melt the substrate to form the melt pool, and P_L is the power lost by reflection, radiation, convection, and etc. Generally, the increasing Si content can decrease the melting point of composite powder, resulting to a decrease in P_p. Correspondingly, the P_s is increased, which in turn leads to an increase in melting height of substrate. As a result, the
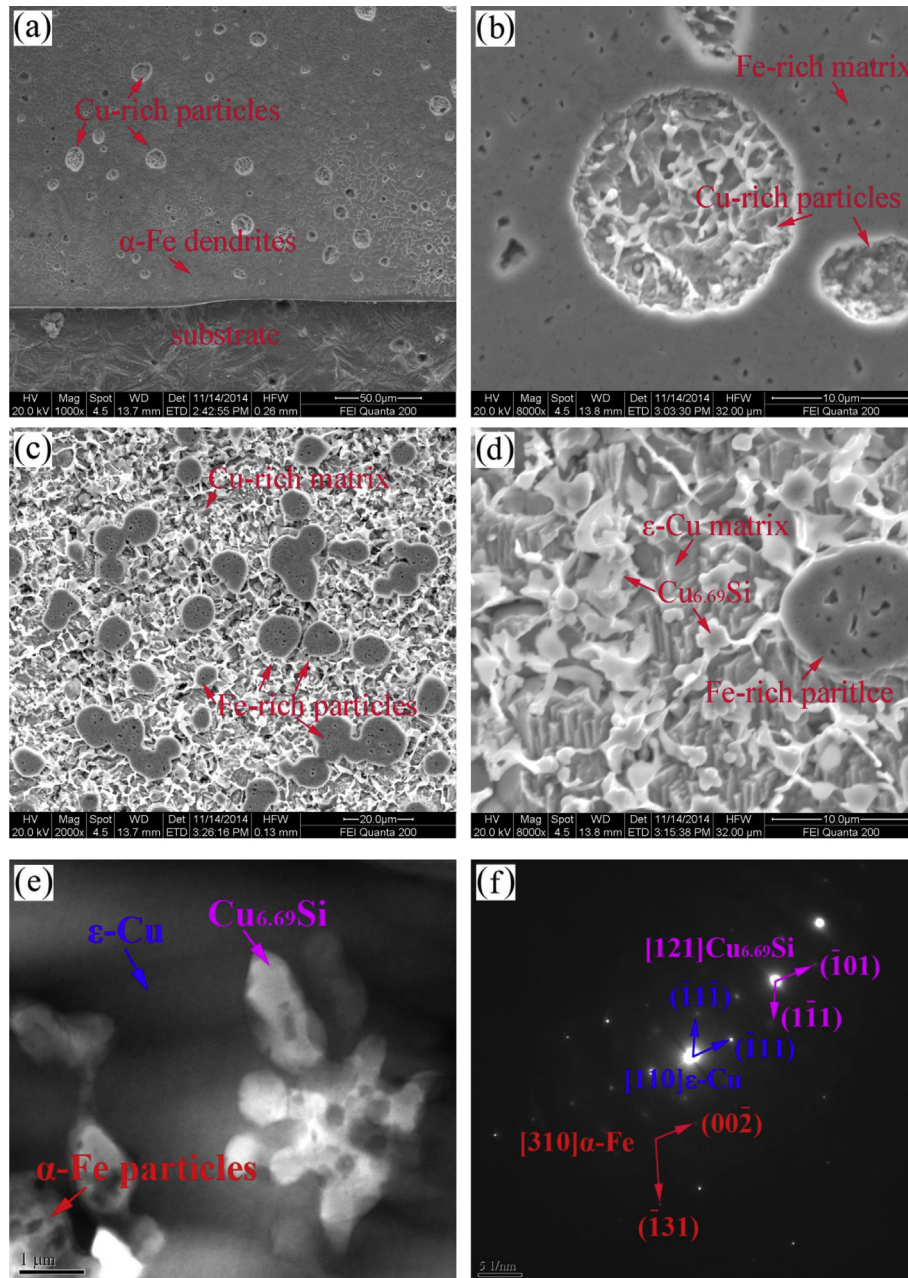

Fig. 4. Microstructure of Fe-rich layer in the $Cu_{55.2}(FeCrC)_{36.8}Si_8$ immiscible composite, (b) magnified image of (a), (c) microstructure of Cu-rich layer in the immiscible composite, and (d) magnified image of (c), (e) TEM images and (f) SAED patterns of the immiscible composite.
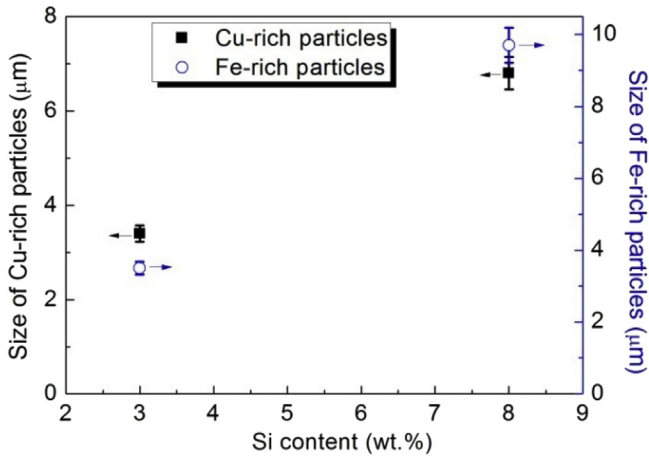
Fig. 5. Effect of Si content on the size of Cu- and Fe-rich particles in the immiscible composites.
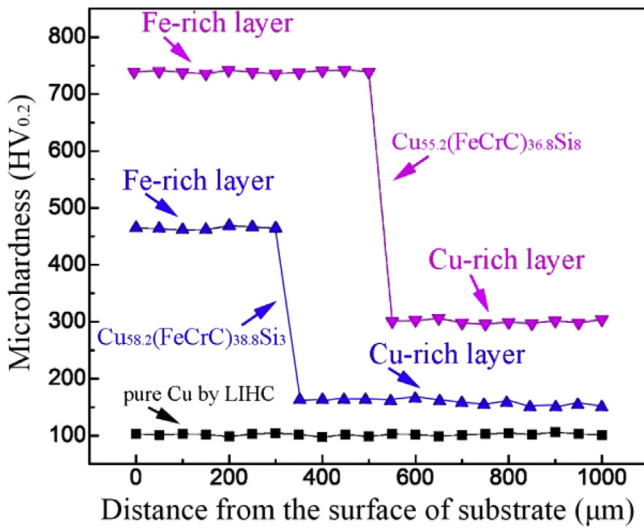

Fig. 6. Microhardness characteristic of the immiscible composites and pure Cu produced by LIHC.

dilution of the immiscible composite is increased from 8.6% to 13.5% so that the more melting of the substrate increases the area of Fe-rich layer (Fig. 2c).

Moreover, once the LPS occurs during LIHC, the L2 as the minor phase can shrink into large amounts of liquid droplets in the Fe-rich lower melt due to minimization surface energy. Similarly, the L1 as the minor phase can also shrink into many liquid droplets in the Cu-rich upper melt. These liquid droplets can move in the liquid matrix, driven by Marangoni motion and Stokes motion. Previous results [15] have shown that the velocity of the liquid droplets induced by Marangoni motion is ~10^4 times faster than that induced by Stokes motion, implying that the Stokes effect can be ignored. For a simple analysis, the velocity of the liquid droplets induced by Marangoni motion is estimated as follows [15]:

$$v_m = \frac{2r_d}{3(3\eta_d + 2\eta_d)} \cdot \frac{\partial \sigma}{\partial T} \cdot G \qquad (3)$$

where r_d is the radius of the liquid droplet, G is the temperature gradient, η_d and η_m are the viscosities of the liquid droplet and the liquid matrix, respectively, and the $\frac{\partial \sigma}{\partial T}$ is the interfacial energy. Furthermore, the viscosity of melt can be described as follows [31]:

$$\eta = 5.7 \times 10^{-6} \frac{\sqrt{M \cdot T_m}}{V_m^{2/3}} \qquad (4)$$

where M is the atom weight, and V_m is the atom volume at temperature T_m. According to the Eq. (4), the viscosity of Si calculated (2.24 cP) is smaller than that of Fe (4.55 cP) and Cu (3.95 cP). Thus, the increasing Si content can decrease the viscosity of melt during LIHC. The velocity of liquid droplets driven by Marangoni motion is increased according to the Eq. (3). Thus, the increasing Si content can obtain higher Marangoni velocity of liquid droplets in the liquid matrix. Li et al. [32] also reported a similar effect of the Ce addition on Marangoni velocity of the Cu-Sn droplets in the Cu-Sn-Bi immiscible alloy. This in turn increases the probability of collision and coalescence of liquid droplets in the liquid matrix. Therefore, the liquid droplets can collide and impinge to form a new larger droplet by the diffusion-coupling mechanism or the gradient induced coupling mechanism [33]. As a result, the Fe- and Cu-rich particles in the Cu$_{55.2}$(FeCrC)$_{36.8}$Si$_8$ immiscible composite present a relatively larger size compared to those in the Cu$_{58.2}$(FeCrC)$_{38.8}$Si$_3$ immiscible composite (Figs. 3–5).

Furthermore, the ε-Cu and α-Fe phases present the index of crystallographic direction [100] and [221] in the Cu$_{58.2}$(FeCrC)$_{38.8}$Si$_3$ immiscible composite, respectively. However, they present the index of crystallographic direction [110] and [310] in the Cu$_{55.2}$(FeCrC)$_{36.8}$Si$_8$ immiscible composite, respectively. Generally, the solid solubility of the Cu in α-Fe phase is negligible at room
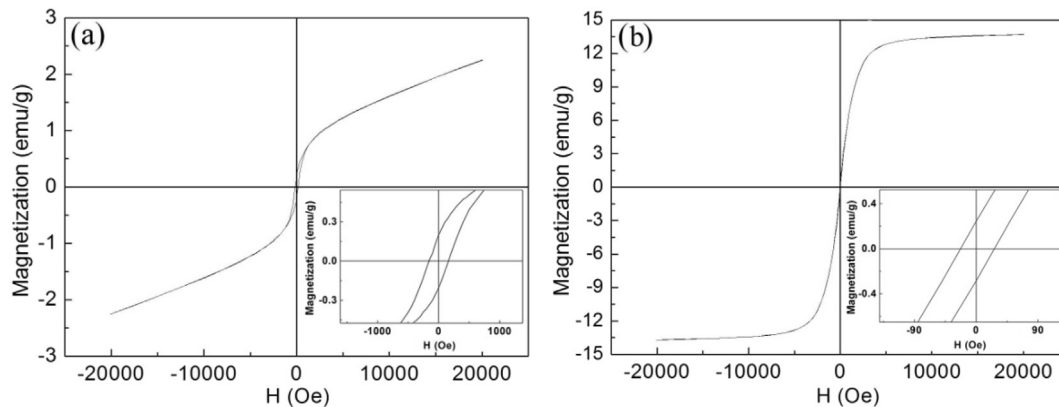

Fig. 7. Magnetic hysteresis loop of the immiscible composites with different Si contents at 300 K: (a) 3 wt% Si, (b) 8 wt% Si.
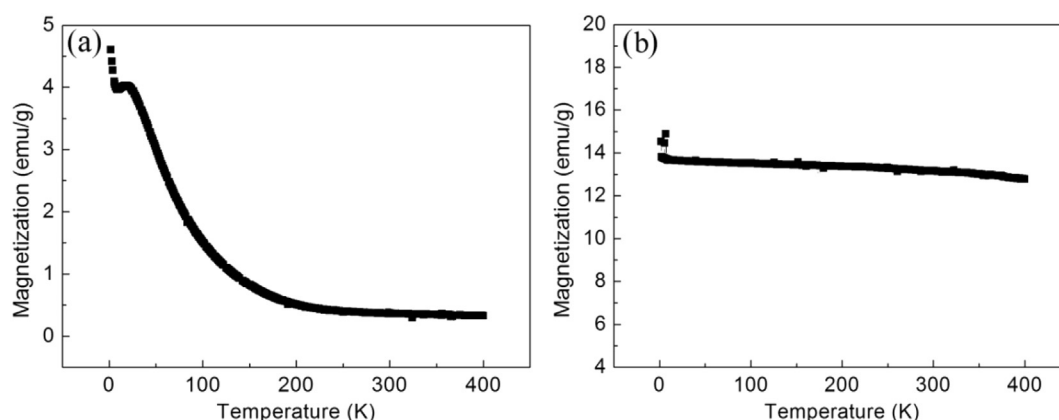
Fig. 8. Temperature dependence of magnetization curve of immiscible composites with different Si contents at a magnetic field of 500 Oe during heating: (a) 3 wt% Si content, (b) 8 wt% Si content.

temperature [26]. Due to high cooling rate during LIHC, the solute trapping can occur [21], resulting in a supersaturated Cu in the α-Fe phase and a supersaturated Fe in the ε-Cu phase. However, as a result of increasing Si content, the supersaturated solid solubility of Cu in the α-Fe particles and matrix decreases from 16.34 wt% and 12.7 wt% to 7.81 wt% and 7.11 wt%, respectively, which is in reasonable accordance with the experimental results from Zhao et al. [8]. Similarly, the supersaturated solid solubility of Fe in the ε-Cu particles and matrix also decreases from 16.3 wt% and 7.19 wt% to 11.47 wt% and 4.26 wt%, respectively. However, the solid solubility of Si in the α-Fe particles and matrix, and ε-Cu particles and matrix increases significantly with the increasing of Si addition. This in turn causes the lattice distortion and non-coherent interface of α-Fe and ε-Cu phases, resulting in different index of crystalline direction and solid solution strengthening. Additionally, large amounts of α-Fe and ε-Cu particles are dispersed in the ε-Cu and α-Fe matrix, resulting in dispersion strengthening. Especially, due to the precipitation of intermetallic compound (IMC) $Cu_{6.69}Si$ precipitations and an increase in diameter of the ε-Cu and α-Fe particles, the microhardness of the $Cu_{55.2}(FeCrC)_{36.8}Si_8$ immiscible composite is strengthened significantly compared to the $Cu_{58.2}(FeCrC)_{38.8}Si_3$ immiscible composite and pure Cu produced by LIHC (Fig. 6).

When the Si content is only 3 wt%, the immiscible composite can not present a saturated magnetization (Fig. 7a). This is because the presence of the paramagnetic contribution of the ε-Cu phase, which has a similar magnetic characteristic to $Fe_{50}Si_{50}$ nanostructured powder produced by a combination of melting and milling process [34]. Especially, when the immiscible composite is heated in the range of 1.9–400 K at 500 Oe, the magnetization of the immiscible composite is reduced significantly to zero at ~200 K shown in Fig. 8a, conforming that the ferromagnetic (FM)-paramagnetic (PM) transformation at Curie temperature lower than 200 K. However, when the Si content is increased to 8 wt%, the immiscible composite presents a characteristic of the saturated magnetization, many be because increasing Si content can increase the area of the FM α-Fe(Si) layer containing 10.36 wt% Si and the diameter of the FM α-Fe(Si) particles containing 17.44 wt% Si, which can be also confirmed by Fig. 8b as a result of almost unchanged magnetization during heating. This is because substitution of Cu atoms by Si atoms in the bcc Fe-rich matrix or particles and the magneto-volume effect results in positive exchange interactions between Fe atoms [35]. The decrease in coercivity in the $Cu_{55.2}(FeCrC)_{36.8}Si_8$ immiscible composite are due to absent precipitation of nano-scaled Fe-rich particles in the Cu-rich matrix

[36]. Obviously, the increasing Si addition can improve the Curie temperature (higher than 400 K) of the immiscible composites.

5. Conclusions

(1) The duplex structure of the $Cu_{58.2}(FeCrC)_{38.8}Si_3$ immiscible composite is mainly composed of many ε-Cu particles embedded within the α-Fe lower dendrites and large amounts of α-Fe particles dispersed within the ε-Cu upper matrix. When the Si addition is increased to 8 wt%, the immiscible composite has a similar duplex structure, while large amounts of intermetallic compounds identified as $Cu_{6.69}Si$ are precipitated within the ε-Cu upper layer.

(2) The increasing Si addition to Cu-Fe-based immiscible composites can increase the area of Fe-rich layer, the size of Fe- and Cu-rich particles, the solid solubility of Si in the α-Fe and ε-Cu phases, while decrease the supersaturated solid solubility of Cu and Fe in the α-Fe and ε-Cu phases. As a result, the microhardness of the Fe- and Cu-rich layers is improved significantly, due to the IMC $Cu_{6.69}Si$ precipitations, and an increase in diameter of the ε-Cu and α-Fe particles.

(3) The $Cu_{58.2}(FeCrC)_{38.8}Si_3$ immiscible composite cannot present a saturated magnetization and is characterized by ferromagnetic (FM)-paramagnetic (PM) transformation during heating. However, the $Cu_{55.2}(FeCrC)_{36.8}Si_8$ immiscible composite presents the saturated magnetization (13.7 emu/g), relatively lower coercivity (24.9 Oe) and higher Curie temperature (larger than 400 K) as a result of the ferromagnetic α-Fe(Si) phase.

References

[1] J. He, J.Z. Zhao, L. Ratke, Solidification microstructure and dynamics of metastable phase transformation in undercooled liquid Cu-Fe alloys, Acta Mater. 54 (2006) 1749–1757.
[2] A. Munitz, A.M. Bamberger, S. Wannaparhun, R. Abbaschian, Effect of supercooling and cooling rate on the microstructure of Cu-Co-Fe alloys, J. Mater. Sci. 41 (2006) 2749–2759.
[3] R.P. Shi, C.P. Wang, D. Wheeler, X.J. Liu, Y. Wang, Formation mechanisms of self-organized core/shell and core/shell/corona microstructures in liquid droplets of immiscible alloys, Acta Mater. 61 (2013) 1229–1243.

[4] I. Ohnuma, T. Saegusa, Y. Takaku, C.P. Wang, X.J. Liu, R. Kainuma, K. Ishida, Microstructural evolution of alloy powder for electronic materials with liquid miscible gap, J. Electron. Mater. 38 (2009) 2–9.

[5] A. Munitz, A. Venkert, P. Landau, M.J. Kaufman, R. Abbaschian, Microstructure and phase selection in supercooled cooper alloys exhibiting metastable liquid miscibility gaps, J. Mater. Sci. 47 (2012) 7955–7970.

[6] J. He, J.Z. Zhao, Behavior of Fe-rich phase during rapid solidification of Cu-Fe hypoperitectic alloy, Mater. Sci. Eng. 404 (2005) 85–90.

[7] S. Zhou, X. Dai, Z. Xiong, C. Wu, T. Zhang, Z. Zhang, Influence of Al addition on microstructure and properties of Cu-Fe-based coatings by laser induction hybrid rapid cladding, J. Mater. Res. 29 (2014) 865–873.

[8] J. Zhao, L. Zhang, Y. Du, H. Xu, J. Liang, B. Huang, Experimental investigation and thermodynamic reassessment of the Cu-Fe-Si system, Metall. Mater. Trans. 40 (2009) 1811–1825.

[9] T. Koziel, Z. Kedzierski, A.Z. Lipiec, K. Ziewiec, The microstructure of liquid immiscible Fe-Cu-based in situ formed amorphous/crystalline composite, Scripta Mater. 54 (2006) 1991–1995.

[10] T. Nagase, M. Suzuki, T. Tanaka, Formation of amorphous phase with crystalline globules in Fe-Cu-Nb-B immiscible alloys, J. Alloy. Comp. 619 (2015) 267–274.

[11] S.B. Luo, W.L. Wang, Z.C. Xia, B. Wei, Phase separation and subsequent solidification of peritectic Fe-Cu-Ge alloys subjected to substantial undercooling processing, J. Alloy. Comp. 717 (2017) 190–196.

[12] Z.C. Xia, W.L. Wang, S.B. Luo, B. Wei, Liquid phase separation and rapid dendritic growth of highly undercooled ternary $Fe_{62.5}Cu_{27.5}Sn_{10}$ alloy, J. Appl. Phys. 117 (2015), 054901.

[13] H.P. Wang, B.C. Luo, T. Qin, J. Chang, B. Wei, Surface tension of liquid ternary Fe-Cu-Mo alloys measured by electromagnetic levitation oscillating drop method, J. Chem. Phys. 129 (2008) 124706.

[14] K. Zhang, X. Bian, Y. Li, C. Yang, H. Yang, Y. Zhang, High-efficiency control of phase separation in Al-based immiscible alloys, J. Alloy. Comp. 639 (2015) 563–570.

[15] C.P. Wang, X.J. Liu, I. Ohnuma, R. Kainuma, K. Ishida, Formation of immiscible alloy powders with egg-type microstructure, Science 297 (2002) 990–993.

[16] T. Koziel, A.Z. Lipiec, J. Latuch, S. Kac, Microstructure and properties of the in situ formed amorphous-crystalline composites in the Fe-Cu-based immiscible alloys, J. Alloy. Comp. 509 (2011) 4891–4895.

[17] T. Nagase, M. Suzuki, T. Tanaka, Formation of nanoglobules with core-shell structure by liquid phase separation in Fe-Cu-Zr-B immiscible alloy, J. Alloy. Comp. 619 (2015) 332–337.

[18] L. Fu, J. Yang, Q. Bi, W. Liu, Combustion synthesis immiscible nanostructured Fe-Cu alloy, J. Alloy. Comp. 482 (2009) L22–L24.

[19] S. Zhou, C. Wu, T. Zhang, Z. Zhang, Carbon nanotube- and Fe_p-reinforced copper-matrix composites by laser induction hybrid rapid cladding, Scripta Mater. 76 (2014) 25–28.

[20] X. Dai, S. Zhou, M. Wang, J. Lei, M. Xie, H. Chen, C. Wang, T. Wang, Effect of substrate types on the microstructure and properties of Cu65Fe35 composite coatings by laser induction hybrid cladding, J. Alloy. Comp. 722 (2017) 173–182.

[21] X. Dai, S. Zhou, M. Wang, J. Lei, C. Wang, T. Wang, Microstructure evolution of phase separated Fe-Cu-Cr-C coatings by laser induction hybrid cladding, Surf. Coating. Technol. 324 (2017) 518–525.

[22] M. Hino, T. Nagasaka, T. Washizu, Phase diagram of Fe-Cu-Si ternary system above 1523 K, J. Phase Equil. 20 (1999) 179–186.

[23] H.R. Jo, J.T. Kim, S.H. Hong, Y.S. Kim, H.J. Park, W.J. Park, J.M. Park, K.B. Kim, Effect of silicon on microstructure and mechanical properties of Cu-Fe alloys, J. Alloy. Comp. 707 (2017) 184–188.

[24] S.B. Luo, W.L. Wang, Z.C. Xia, Y.H. Wu, B. Wei, Solute redistribution during phase separation of ternary Fe-Cu-Si alloy, Appl. Phys. A 119 (2015) 1003–1011.

[25] S. Zhou, Y. Huang, X. Zeng, Q. Hu, Microstructure characteristics of Ni-based WC composite coatings by laser induction hybrid rapid cladding, Mater. Sci. Eng. 480 (2008) 564–572.

[26] A. Munitz, Liquid separation effects in Fe-Cu alloys solidified under different cooling rates, Metall. Mater. Trans. B 18 (1987) 565–575.

[27] Y.Z. Chen, F. Liu, G.C. Yang, X.Q. Xu, Y.H. Zhou, Rapid solidification of bulk undercooled hypoperitectic Fe-Cu alloy, J. Alloy. Comp. 427 (2007) L1–L5.

[28] Y.Y. Chuang, R. Schmid, Y.A. Chang, Thermodynamic analysis of the iron-copper system I: the stable and metastable phase equilibria, Mater. Trans. A 15 (1984) 1921–1930.

[29] H.P. Gedda, J. Powell, G. Wahlstrom, W.B. Li, H. Engstrom, C. Magnusson, Energy redistribution during CO_2 laser cladding, J. Laser Appl. 14 (2002) 78–82.

[30] S. Zhou, X. Dai, X. Zeng, Effects of processing parameters on structure of Ni-based WC composite coatings during laser induction hybrid rapid cladding, Appl. Surf. Sci. 255 (2009) 8494–8500.

[31] E.N. Andrade, Theory of viscosity of liquids, Philos. Mag 17 (1934) 497–698.

[32] J. Li, B. Ma, S. Min, J. Lee, Z. Yuan, L. Zang, Effect of Ce addition on macroscopic core-shell, Mater. Lett. 64 (2010) 814–816.

[33] H. Tanaka, A new coarsening mechanism of droplet spinodal decomposition, J. Chem. Phys. 103 (1995) 2361–2364.

[34] J.F. Piamba, G.A. Perez Alcazar, Effect of disorder on the structural and magnetic properties of the Fe50Si50 nanostructured system, J. Alloy. Comp. 643 (2015) S297–S301.

[35] T. Mashimo, X. Huang, X. Fan, K. Koyama, M. Motokawa, Slater-pauling curve of Fe-Cu solid solution alloys, Phys. Rev. B 66 (2002), 132407.

[36] B.N. Mondal, A. Basumallick, P.P. Chattopadhyay, Effect of isothermal treatments on the magnetic behavior of nanocrystalline Cu-Ni-Fe alloy prepared by mechanical alloying, J. Magn. Magn Mater. 309 (2007) 290–294.